The development of enabling technologies for producing active interrogation beams

Cite as: Rev. Sci. Instrum. **81**, 103304 (2010); https://doi.org/10.1063/1.3488354
Submitted: 17 May 2010 • Accepted: 16 August 2010 • Published Online: 25 October 2010

Thomas J. T. Kwan, Richard E. Morgado, Tai-Sen F. Wang, et al.

The development of enabling technologies for producing active interrogation beams

Thomas J. T. Kwan,[1] Richard E. Morgado,[1] Tai-Sen F. Wang,[1] B. Vodolaga,[2] V. Terekhin,[2] L. M. Onischenko,[3] S. B. Vorozhtsov,[3] E. V. Samsonov,[3] A. S. Vorozhtsov,[3] Yu. G. Alenitsky,[3] E. E. Perpelkin,[3] A. A. Glazov,[3] D. L. Novikov,[3] V. Parkhomchuk,[4] V. Reva,[4] V. Vostrikov,[4] V. A. Mashinin,[5] S. N. Fedotov,[5] and S. A. Minayev[5]
[1]*Los Alamos National Laboratory, Los Alamos, New Mexico 87544, USA*
[2]*All-Russia Scientific Research Institute of Technical Physics, Snezhinsk, Russia*
[3]*Joint Institute of Nuclear Research, Joliot-Curie 6, 141980 Dubna, Moscow Region, Russia*
[4]*Budker Institute of Nuclear Physics (BINP), Av. Lavrent'ev, 630090 Novosibirsk, Russia*
[5]*Research Firm IFI, Moscow, Russia*

(Received 17 May 2010; accepted 16 August 2010; published online 25 October 2010)

A U.S./Russian collaboration of accelerator scientists was directed to the development of high averaged-current (~1 mA) and high-quality (emittance ~15 πmm mrad; energy spread ~0.1%) 1.75 MeV proton beams to produce active interrogation beams that could be applied to counterterrorism. Several accelerator technologies were investigated. These included an electrostatic tandem accelerator of novel design, a compact cyclotron, and a storage ring with energy compensation and electron cooling. Production targets capable of withstanding the beam power levels were designed, fabricated, and tested. The cyclotron/storage-ring system was theoretically studied and computationally designed, and the electrostatic vacuum tandem accelerator at BINP was demonstrated for its potential in active interrogation of explosives and special nuclear materials.
 [doi:10.1063/1.3488354]

I. INTRODUCTION

Accelerator scientists and nuclear physicists from Russian Institutes and an American National Laboratory have worked together since 2004 to develop several accelerator variants capable of producing high-quality, megavoltage, multimilliampere proton beams. An accelerator system consisting of a compact cyclotron and a storage ring with energy compensation and electron cooling was studied and designed. Experiments were conducted using the proton beam from an advanced electrostatic tandem accelerator at BINP to demonstrate the feasibility of nuclear resonance absorption as a method of active interaction of concealed high explosives and special nuclear materials. The proton beam from the accelerator is required to produce the secondary gamma ray and neutron active interrogation beams for interrogation. Participants included the All Russian Institute for Technical Physics (VNIITF) in Snezhinsk, the Joint Institute of Nuclear Research (JINR) in Dubna, the Budker Institute of Nuclear Physics (BINP) in Novosibirsk, the Research Firm IFI of Moscow, and Los Alamos National Laboratory. We report on the results of the project that was concluded in 2008.

II. RATIONALE

The accelerator technologies considered were those capable of producing resonant gamma-ray beams from proton capture reactions suitable for nuclear resonance absorption (NRA) and gamma-ray resonant scattering (GRS), as well as monoenergetic gamma ray and neutron beams to induce fission in highly enriched uranium. These technologies included a high-current electrostatic variant, the vacuum insulated tandem accelerator (VITA) at the Budker Institute of Nuclear Physics (BINP), two variants of a compact cyclotron at the Joint Institute of Nuclear Research (JINR), and a storage ring with an internal target, energy compensation, and electron cooling, at BINP and JINR.

A. NRA for explosives detection

NRA in the nitrogen component of high explosives requires a very narrow spectrum of gamma rays, centered at 9.17 MeV. One method of producing such a spectrum utilizes the proton-capture resonant reaction

$$^{13}\mathrm{C}(p,\gamma)^{14}\mathrm{N}$$

in which a beam of well-defined 1.75 MeV protons are captured in carbon-13 to form the 9.17 MeV excited state of nitrogen-14. The recoiling nitrogen-14 nucleus subsequently decays in flight, emitting a Doppler-shifted 9.17 MeV gamma ray. At 80.6° with respect to the recoiling nitrogen-14, the emitted gamma-ray energy has Doppler-shifted an energy equivalent to two nuclear-recoils: one nuclear recoil energy that is lost during emission and an additional nuclear recoil energy required for subsequent resonant absorption in nitrogen.

The detection of explosives utilizes the prominent and narrow (122 eV) gamma-ray resonance absorption via the inverse reaction

$$^{14}\mathrm{N}(\gamma,p)^{13}\mathrm{C}.$$

This results in a very strong absorption of gamma rays in nitrogen at precisely 9.17 MeV. Since most high explosives contain high percent weight compositions of nitrogen, this

TABLE I. Gamma-ray yields from (p,γ) reactions in selected target.

Target nuclei	Daughter nuclei	Gamma-ray energy (keV)	Width of spectrum (eV)	Level energy (keV)	Proton energy (keV)	Gamma-ray yield per proton
^{13}C	^{14}N	8062	2.30×10^{4}	8062	551	9.40×10^{-9}
^{13}C	^{14}N	8776	4.10×10^{5}	8776	1320	1.10×10^{-8}
^{13}C	^{14}N	9172.25	1.20×10^{2}	9172.25	1747.6	6.00×10^{-9}
^{11}B	^{12}C	12131.1	3.00×10^{5}	16570	675	4.10×10^{-9}
^{11}B	^{12}C	12791.1	1.10×10^{6}	17230	1388	2.60×10^{-9}
^{11}B	^{12}C	17230	1.10×10^{6}	17230	1388	2.40×10^{-8}
^{11}B	^{12}C	4439	3.00×10^{5}	16570	675	4.10×10^{-9}
^{15}N	^{12}C	4439	2.2×10^{3}	16105	898	7.0×10^{-8}
^{15}N	^{12}C	4439	7×10^{4}		1640	$\sim1\times10^{-6}$

method provides a very penetrating probe emanating from a point source that is specific to nitrogen and inherently imaging. Several variants based on the method successfully demonstrated explosives detection in the early 1990s.[1–3]

B. GRS for explosives detection

The gamma-ray scattering (GRS) method, unlike NRA, requires neither the narrow energy spectrum of gamma rays nor the well-defined proton beam emittance to produce it. GRS may be the only resort for explosive detection when access is limited to one side of the interrogated object.

In the GRS version the signal is derived from the elastically scattered resonant gamma rays from the ^{14}N(γ,γ') ^{14}N reaction in nitrogen. The cross section for resonant scattering is a fraction (0.05) of that of resonant absorption but a significant advantage of GRS is that there is *no need* to shape an extremely narrow spectrum of gamma rays, as the scattering medium serves as the "analyzer" for the resonant component in the energy spectrum.

C. Radiography and photofission using monoenergetic gamma-ray beams

The same proton beams can also produce intense monoenergetic gamma-ray beams utilizing (p,γ) and $(p,\alpha\gamma)$ reactions in selected targets for other applications, such as dual-energy radiography and the detection of special nuclear material (SNM) via photofission. Neutron beams from (p,n) reactions in low-Z targets can also be produced and used to induce fission in SNM. The estimated yields of monoenergetic gamma rays from (p,γ) reactions in selected targets are shown in Table I.

The ^{19}F$(p,\alpha\gamma)$ ^{16}O reaction is particularly interesting as a source of monoenergetic gamma rays.[4,5] The dependence of the relative yield of 6 and 7 MeV gamma rays from the excited states of oxygen-16 as a function of proton energy is shown in Fig. 1. These gamma rays are suitable for penetrating dual-energy radiography of dense materials or could be used to produce photofission in SNM while reducing the overall dose to the contents of the object being screened than would be the case for bremsstrahlung beams.

III. ENABLING TECHNOLOGIES

A. Compact cyclotron as a proton source for active interrogation

1. High-current, low-quality beam proton source

Earlier investigations of the beam dynamics in a cyclotron with an external H^- source resulted in the following characteristics:[6]

- Maximum current (~1.8 MeV) 2.2–2.5 mA,
- Transverse emittances: 150–300 πmm mrad,
- Energy spread, $\Delta E/E$: $\pm 8\%$.

Although these beam parameters did not meet the stringent proton source requirements for NRA due to the narrow resonance width, this cyclotron design is adequate as a source for the GRS method and for the production of monoenergetic gamma ray and neutron interrogation beams as a standalone system as described in the previous section.

2. Neutron interrogation beam based on a compact cyclotron

The compact high-current cyclotron accelerator of protons designed by JINR was originally intended for producing gamma rays of sufficient quality for NRA. As a standalone

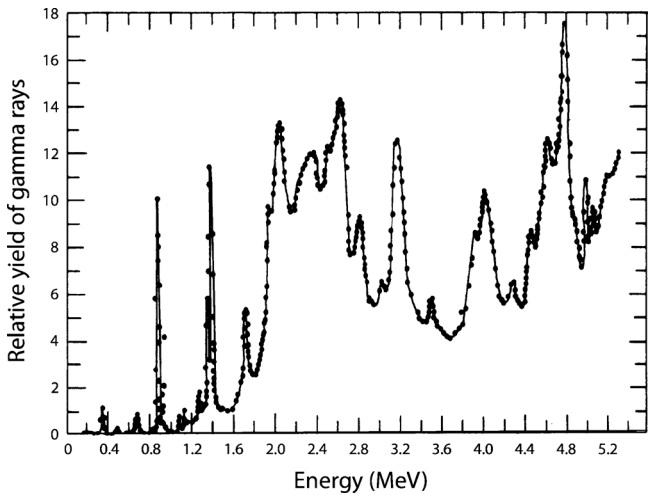

FIG. 1. Gamma-ray yield vs proton energy for the ^{19}F$(p,\alpha\gamma)$ ^{16}O reaction (Ref. 5).

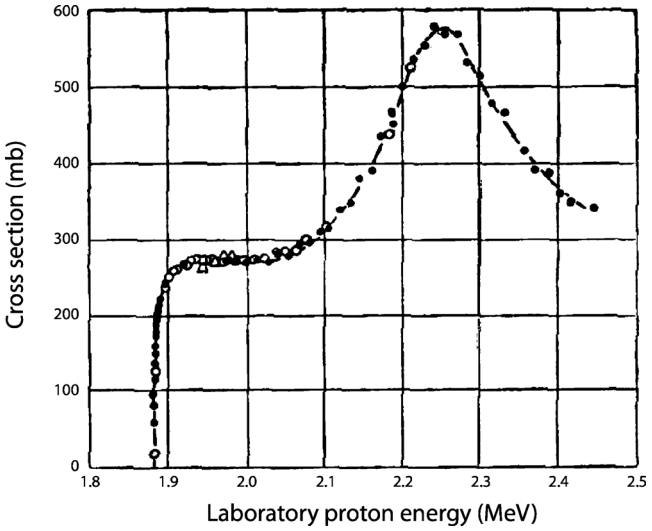

FIG. 2. Total cross section for ^{7}Li(p,n) ^{7}Be from threshold to 2.4 MeV (Ref. 7). Relative error in cross section is ±1%, and absolute error is estimated to be ±5%.

system it was determined to be unable to meet the requirements for NRA. However, it is capable of producing neutron beams as a stand-along source for detecting SNM.

The cross section of reaction for the reaction ^{7}Li(p,n) ^{7}Be from a threshold proton energy of 1.881 MeV up to ~2.4 MeV is depicted in Fig. 2.

The energy distribution of the neutrons (s^{-1} keV^{-1}) from a thick lithium target at various angles in 5° steps beginning from 0° (upper curve) produced by 10 mA protons at 1.92 MeV is depicted in Fig. 3.

B. Low-current, high-quality-beam proton source

To achieve the stringent NRA requirements of a 1.747 MeV proton beam with an intensity of several milliamperes and as small as possible energy spread and angular divergence,[1] a compact isochronous cyclotron with internal H^- ion source and current of ~200 μA was considered as an injector into a storage ring.[8,9]

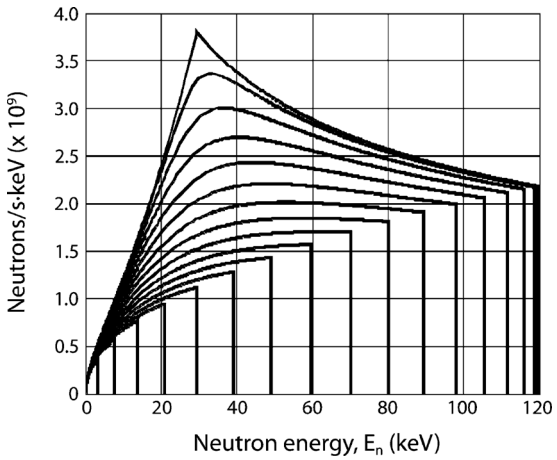

FIG. 3. Energy distribution of the neutrons at various angles in 5° steps (Ref. 8) from a thick lithium target from the incidence of a 10 mA proton beam at an energy of 1.92 MeV. The top curve is at 0°.

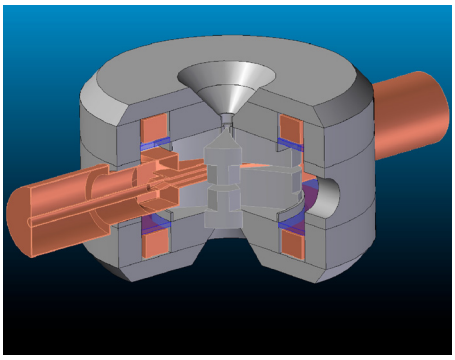

FIG. 4. (Color online) Magnet and rf structures.

An internal ion source capable of delivering 6 mA of H^- was examined. A delimiting diaphragm on the first turn reduced the transverse emittances and the energy spread to NRA acceptable levels at the expense of a 30-fold reduction in average captured beam current from 6 mA to 200 μA.

1. Basic cyclotron parameters

The general view of the cyclotron magnet and rf structures are shown in Fig. 4. Cyclotron parameters are given in Table II. The fourfold-type magnet with all-round yoke cyclotron is shown in Fig. 4. Magnet parameters are given in Table III. The choice of magnetic field strength (0.64 T) was a compromise: the higher the field, the smaller the cyclotron and the larger the space-charge limit due to increased axial focusing. On the other hand, turn separation is decreased along with extraction efficiency.

The radio frequency (rf) system consists of two resonators with two 45° dees located in opposite valleys and with two resonance lines supplied by feeders and rf voltage and phase stabilization and control. The ~39 MHz frequency corresponds to the fourth harmonic of the ion orbit frequency. The accelerating voltage amplitude is $U=60$ kV and the peak energy gain per turn is $\Delta W=4U$. The dissipated power in each resonator is ~5 kW. To accelerate the 0.2 mA H^- beam, the internal ion source[10] has to produce ~2 mA and be small enough to be placed in the compact cyclotron central region.

When the cyclotron is used as an injector, the system consists of a compact cyclotron, a beam delivery system (BDS), and a storage ring.[9] The main criteria included good

TABLE II. Cyclotron parameters.

Parameter	Value
Type of ion	H^-
Injection energy (keV)	30
Extraction energy (keV)	1747
Average magnetic field (T)	0.64
Number of sectors	4
Number of dees	2
Betatron frequencies (Qr,Qz)	1.1, 0.85
Angular span of dees (deg.)	45
rf voltage (kV)	60
Orbital frequency (MHz)	9.76
Harmonic number	4

TABLE III. Magnet parameters.

Parameter	Value
Magnet height	89 cm
Magnet outer radius	70 cm
Pole outer radius	35 cm
Final orbit radius	30 cm
Hill field at final radius	1.35 T
Valley field	0.2 T
Hill gap	3 cm
Valley gap	40 cm
Sector angular width	10°–30°
Power consumption	10 kW

centering, the highest energy gain in the accelerating gaps, maximum transmission, and the best possible beam quality at the final energy. Simulation of the interface between the cyclotron and the storage ring was performed in order to provide the required intensity and beam quality for injection into the storage ring.

C. BDS

Dedicated structure elements in the injection channel provided dispersion control at the storage-ring injection. The optical elements were chosen to regulate the beam parameters at the target point (beta functions and dispersion). By adjusting the corresponding parameters of the cyclotron and the BDS, the required intensity and beam quality for injection into the storage ring were provided.

Figure 5 depicts the layout of the cyclotron, the BDS with the structure elements mentioned above, and the storage ring. H^- ions from the cyclotron strike charge-exchange target 1 ($H^- \rightarrow H^0$) and, subsequently, charge-exchange target 2($H^0 \rightarrow H^+$). The dispersion function at target 2 is controlled to provide the proper correlation between the particle momentum and horizontal position needed for injection into the storage ring. Two triplets and a bending magnet were selected to satisfy the majority of the requirements.

Estimation of the BDS parameters requires knowledge of the energy dispersion function D and its derivative D' along the beam central trajectory at the exit of the cyclotron. To define those parameters, the dependence of the particle energy on its transverse horizontal displacement from the central trajectory was calculated at two successive points

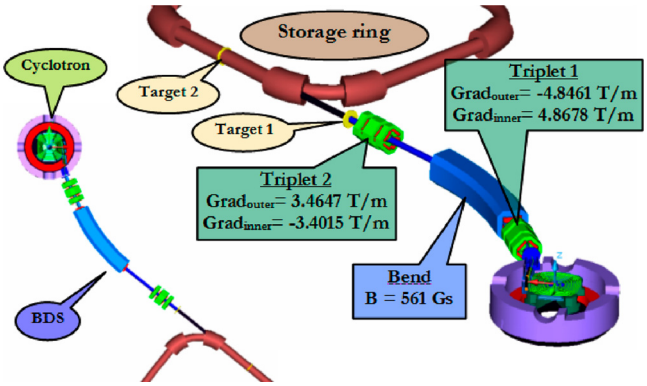

FIG. 5. (Color online) General view of the facility.

TABLE IV. Beam characteristics at the BDS entrance at two intensities.

Intensity (μA)	100	260
Effective horizontal emittance (πmm mrad)	24.2	33
Uncorrelated horizontal emittance (πmm mrad)	3.1	4.9
Energy dispersion function (cm)	14.3	15.3
Energy spread (keV)	31	34
Axial emittance (πmm mrad)	3.2	7.2
Longitudinal emittance (πmm keV)	155	177

along the trajectory. The results obtained at the BDS entrance, summarized in Table IV, show the impact of the space charge on the beam quality. The results were used for particle tracing through the BDS to the injection point in the cooling ring.

In order to eliminate a mismatch between the injection parameters and the beam, i.e., beam widening in the ring, the necessary energy dispersion of the beam (Fig. 6) was produced in the injection channel. The improved qualities of the injected beam, compared to the previous case, permit a substantial increase (by a factor of 4, up to ~40%) in the intensity of the particles captured into the ring.

D. High-luminosity proton storage ring with electron cooling

The role of the proton storage ring is to accumulate and condition the beam for NRA application. To provide the beam quality required for gamma-ray production, electron cooling[11,12] is invoked to decrease the six-dimensional phase space of the proton beam from the accelerator and to mitigate the degradation of beam quality due to interactions with the gamma-ray-production target. In the following, we summarize two investigations: an estimation of the storage-ring requirements for a luggage interrogation system based on a conventional storage-ring design with an external production target[13,14] and a study of several novel ideas in the storage-ring design with an internal production target.[15]

1. Requirements for a conventional design with an external target

In this section, we investigate the requirements for a storage ring with an external target for a variant of a luggage

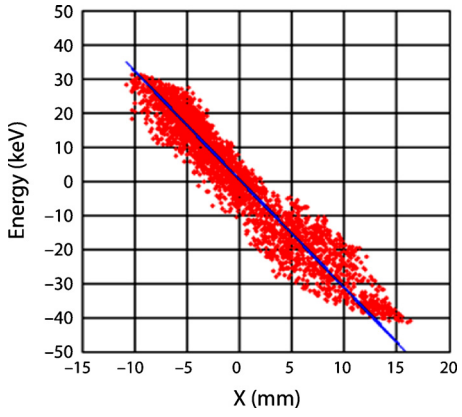

FIG. 6. (Color online) Estimate of dispersion at storage-ring injection point, 130 μA beam current.

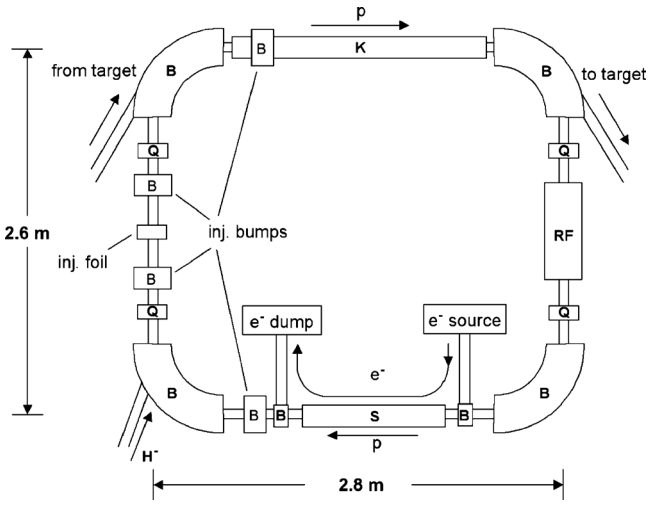

FIG. 7. Layout of the model storage ring.

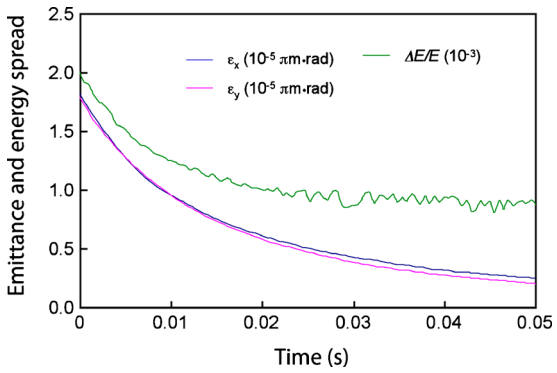

FIG. 8. (Color online) The emittance and the energy spread of the proton beam during the first 0.05 s of cooling.

inspection system using a tomographic imaging approach similar to what was considered in earlier LANL experiments.[16] It is assumed that at each luggage inspection station, four pieces of luggage are interrogated on a platform in a one-bag-per-quadrant arrangement. Each bag is placed on a turntable to rotate the luggage in four 90° intervals and to translate the luggage vertically in four increments. For each vertical step, the luggage is scanned through four rotations of one rotation per second. Assuming a loading time of 8 s, the system is expected to achieve an inspection rate of four bags every 24 s.

Each inspection station includes an array of 64 gamma-ray detectors per quadrant. In the absence of any nitrogen-rich material, each detector should receive about 400 gamma rays per view. At the yield of 0.63×10^{-8} gamma rays per proton, this will require a proton beam that can deliver approximately 1.6×10^{13} protons per pulse.

Accelerated protons are injected into the storage ring, stored, and cooled to achieve the required emittance. When the luggage is positioned and the required beam quality has been achieved, the proton beam is ejected from the storage ring and transported to the gamma-ray-production target. The interaction of protons with the target increases the emittance and decreases the energy of the protons. The increase of the transverse beam emittance in a 20 $\mu g/cm^2$ carbon foil per transit is $\delta\varepsilon\approx3.17$ πmm mrad $\approx0.2\varepsilon_0$, where $\varepsilon_0\approx15$ πmm mrad, which is the upper limit of the beam emittance for a 0.5 cm radius spot with a divergence less than 3 mrad. After exiting the foil, protons are returned to the storage ring, accelerated, and cooled for the next interrogation.

A conceptual storage-ring design is depicted in Fig. 7, showing the layout of the major ring elements. The ring is 10 m in circumference and has four straight sections. Focusing is accomplished by four combined-function bending magnets having a field intensity of 0.375 T, a field index of -1.58, and with edge-pole faces that are normal to the beam line. The horizontal and vertical betatron tunes are 1.63 and 1.24, respectively. Space is reserved in the straight sections for up to four 10-cm-long trim quadrupoles. The cooling section, located in one of the straight sections, has a 0.9-m-long solenoid for providing an axial magnetic field up to 5kG. A 1.5-m-long fast kicker, located in another straight section, is to be operated at 5 kV per plate for a total voltage of 10 kV for beam extraction and injection. A carbon foil and four injection bump magnets are used to facilitate both the initial injection and the reinjection of protons from the target. A ferrite-loaded rf cavity operates at the first and the second harmonics of the proton revolution frequency (1.835 and 3.67 MHz) with maximum voltages of 300 and 100 V, respectively. The rf field is used to compensate the proton energy loss due to the proton-target interaction as well as to maintain the longitudinal bunching of the protons. A single-bunch time structure is sustained in the ring by the rf field at the fundamental harmonic. A gap of more than 130 ns can be maintained prior to the ejection of protons to accommodate a clean extraction by a faster kicker with a moderate rise time less than 120 ns. The use of dual harmonics in the rf cavity enhances the bunching factor and reduces the maximal transverse coherent tune shift by decreasing the peak current at bunch center without losing the averaged proton beam current.

Cooling time is estimated using the lattice functions computed from the program MAD-X (Ref. 17) as an input to the program BETACOOL (Ref. 18) for 0.2 A of electron beam current and 5 kG of solenoid field in the model ring lattice structure. For the increments of 20% in the transverse beam emittance and 100% in energy spread due to the beam-foil interaction ($\Delta E\approx1.9$ keV per traversal of the target), BETACOOL gives about 0.004 s to cool the transverse emittance back to 15 πmm mrad and about 0.02 s to cool the energy spread down to $\Delta E/E\approx1\times10^{-3}$, as shown in Fig. 8. The corresponding average cooling rate is about 35 s^{-1}, limiting the maximal repetition rate of the storage ring to 50 Hz.

In estimating the number of storage rings needed for our nominal explosive detecting system under study, we first notice that the most obvious limitation on the accumulated protons in a storage ring is the space-charge effect, which is roughly given by

$$N=\varepsilon_x\Delta Q_x\frac{4\pi\beta^2\gamma^3}{r_p}, \tag{1}$$

where ΔQ_x is the maximum allowed incoherent betatron tune-shift, ($\Delta Q_x\sim0.25$ for rapid beam loss), $\varepsilon_x=\theta_x^2\beta_x=\sigma_x^2/\beta_x$ is the rms beam emittance, $\beta=v/c$, $\gamma=(1-\beta^2)^{-1/2}$, v

is the velocity of a beam particle, and r_p is the classical radius of a proton. Then, either by directly applying Eq. (1) or by using the equation to scale from the storage rings MIMAS, PSR, and the storage ring at BINP, we conclude that the maximum number of protons that can be stored in our model ring is between 10^{10} and 10^{11}.[14] If we also assume a 20 $\mu g/cm^2$ carbon foil is used for the target and 0.02 s is needed for beam cooling, we estimate that four rings are needed to achieve a 1.6×10^{13} proton/second average beam current at the target.

Thus, a single storage ring is unlikely to provide the required proton beam intensity, but it is possible that no more than a few storage rings per inspection station will provide a practical luggage inspection complex with more than ten inspection stations.

For practical applications, it is highly desirable to produce all the required flux using only one storage ring, which will require novel design concepts, as discussed in the next section. It should be noted that the system discussed above is limited to the use of an external target, and we have not considered the proton beam intensity limitation in the storage rings due to collective instabilities, which might be more stringent than the limit imposed by the space-charge effect.

2. Storage-ring designs based on novel ideas and an internal target

To increase the gamma ray production, one would like to store as many protons as possible in the storage ring and locate the target inside the ring to maximize the interactions between the beam and target. The continuous traversal of the proton beam through the target rapidly degrades proton beam quality, thus requiring an electron beam current greater than the proton beam current to achieve fast cooling. New ideas are being sought on how to operate the storage ring with both the proton and the electron beam currents above their individual and possibly even their net space-charge limit. Further studies are required to assess the feasibility of these new ideas.

Two approaches addressing the space-charge limit are possible. The first uses a special magnetic structure with a strong longitudinal magnetic field resembling a tokamak or a stellarator.[19] The protons are magnetized and move along the lines of force of the longitudinal magnetic field. Proton motion can be described as two types: a fast cyclotron rotation around the lines of force and a slow drift from one magnetic line of force to another. Such a dynamic proton beam can be described by two beta functions. One is responsible for strong focusing and has a small value

$$\beta_s = \frac{\gamma\beta m_p c^2}{eB}.$$

If the magnetic field $B=10$ kG, e.g., $\beta_s=20$ cm.

The other β-function is larger

$$\beta_{\max} = R_{\mathrm{av}}/Q_\perp,$$

where $Q_\perp$ is a drift frequency around the magnetic axis. For $Q_\perp=0.2$, the maximum beta-function would be $\beta_{\max}=700$ cm. The proton beam consists of many small beam components comprising the larger whole beam. For an angular spread ~1 mrad, the rotation radius around the force line at 10 kG magnetic field will be $a_p=\beta_s\theta_{\max}=0.2$ mm, and the total proton beam size $\beta_{\max}\theta_{\max}=0.7$ cm.

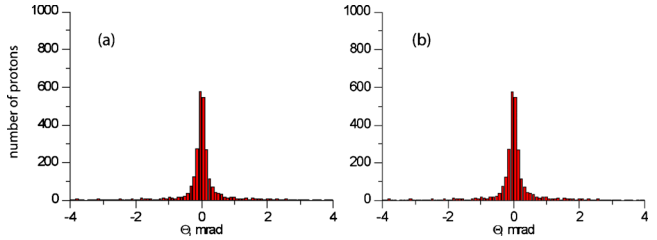

FIG. 9. (Color online) Monte Carlo simulations showing angular spread of the proton beam with cooling and target degrading processes: (a) $\Delta t=147$ μs and (b) $\Delta t=750$ μs. The target thickness is 4.0×10^{15} cm^{-2} and the initial proton beam is cooled. The electron current is 1.5 A and the radius of the electron beam is 0.4 cm. Multiple scattering is described by the Rutherford model.

The second approach to mitigate the space-charge effect is to neutralize the net negative space charge due to the excessive electron beam current with the help of the accumulation of ions from the residual gas and/or target ionization. This is studied in conjunction with the electron cooling. Figure 9 shows the Monte Carlo simulation result of the combined processes in the target and electron cooler. Figure 10 depicts the interaction of the proton beam with the target without cooling. It is shown that cooling enables a practically "quasistationary" process without degradation of beam quality. The absence of the cooler leads to rapid degradation of the proton beam for even a small target density.

If the electron cooling effectively compensates the beam-quality degradation due to interaction with the target, then the luminosity can be determined

$$L = \frac{I_p}{e} n_a = 1.6\times10^{34}\ \mathrm{cm^{-2}\ s^{-1}}$$

for a target density $n_a=5\times10^{15}$ cm^{-2} and proton current $I_p=0.5$ A, corresponding to a gamma-ray flux of about 5.5×10^8 s^{-1} ($\sigma\gamma=3.5\times10^{-26}$ cm^{-2}). This optimistic estimation of the ultimate luminosity requires detailed research and development and the investigation of prototypes of many elements.

It is maybe unrealistic to cool with an electron beam current in the range of amperes, but we can conceive that a practical cooling system with a few hundred milliamps of electron beam current could be possible. But even at the lowered electron beam current, the net charge in the system

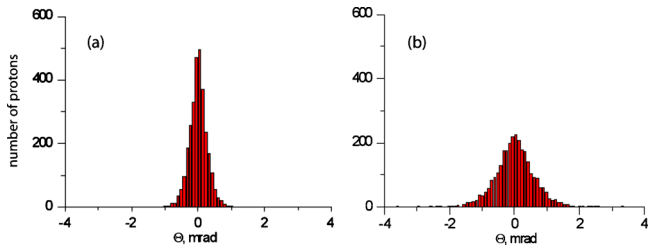

FIG. 10. (Color online) Monte Carlo simulations showing angular spread of the proton beam due to a 1.0×10^{15} cm^{-2} target: (a) $\Delta t=73$ μs and (b) $\Delta t=370$ μs. The initial proton beam is cooled. Multiple scattering is described by the Rutherford model.

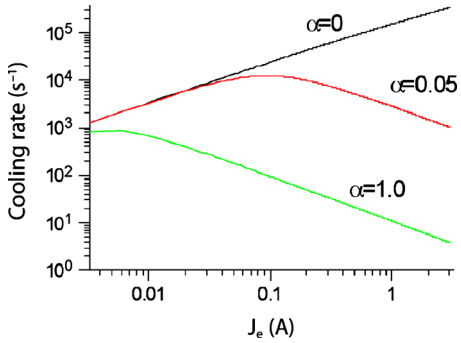

FIG. 11. (Color online) Cooling force vs electron current for different values of the neutralization factor (α=1.0 means no neutralization).

could be negative, and neutralization by introducing ions is required to ameliorate space-charge effects in the electron beam. The secondary ions not only decrease the effect of the space-charge field on the electron motion but also allow electron beams with higher intensity. Figure 11 compares the cooling rates for different levels of the neutralization parameter. If the non-neutralized electric field is more than 0.2% of the maximum value there are significant problems in obtaining maximal parameters.

One of the limitations to achieving a stable compensated state is the appearance and progression of different beam-driven instabilities. A rough criterion for compensated-state stability is a small value of oscillation phase advance of the electron drift motion during time of flight through the cooling region

$$\omega_d \frac{l_{\text{cool}}}{\beta c} < 1.$$

It gives the limit of the maximum possible density of electron beam, namely

$$n_e < \frac{B\beta}{2\pi e l_{\text{cool}}} = \frac{(2\times 10^4)(6.5\times 10^{-2})}{2\pi(4.8\times 10^{-10})(100)} \approx 4\times 10^9 \ \text{cm}^{-3}.$$

Although this condition is not absolute, its realization leads to a short length of the electron beam and a large value of the magnetic field. The coherent processes determine the compensation stability. The experiences with compensated proton and electron beams at BINP have shown that stable states are possible but this problem may be finally solved only by experiments.[20]

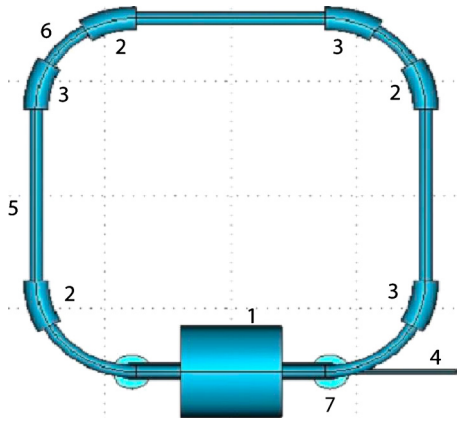

FIG. 12. (Color online) Sketch of storage-ring vacuum chamber. (1) Target for the generation of gamma rays (at the same time it is the target for charge exchange injection), (2) electron gun section, (3) collector section, (4) injection section, (5) cooling section, (6) bending section, and (7) pumping section.

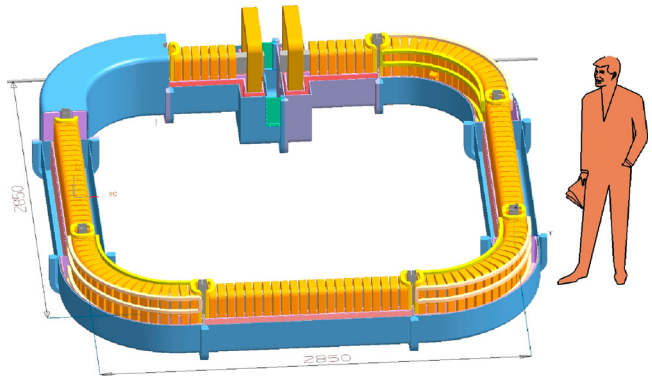

FIG. 13. (Color online) Three-dimensional sketch of storage ring with longitudinal magnetic field.

Figures 12 and 13 show the structure of the storage ring with the longitudinal magnetic field. The H^- ions from the cyclotron are first stripped to neutral H^0 that are injected into the strong magnetic field along the injection line 4. The target (1) for charge exchange from H^0 to protons H^+ also generates the resonance x-rays. The protons travel in the clockwise direction. The electron beam is produced in three electron gun areas (2). The electrons and protons move together in straight sections (5) and are absorbed in the collector in region (3). The dipole magnet is used to separate the proton and electron beams. An example of such a separation scheme is shown in Fig. 14. The transverse magnetic field in the dipole shifts the magnetic force line from the magnetic axis. The proton beam moves in the orbit plane since the transverse (dipole) field is compensated by centrifugal force $\gamma\beta m_p c^2/R$. Electrons, 1836 times lighter, follow the force line upwards. At the same time electrons for cooling in the next straight section can be brought into the orbit plane from below. The preliminary parameters of such storage ring are shown in the Table V.

3. Conclusions on storage-ring studies

We have presented two studies on the storage-ring requirements for NRA applications. First, we estimated the storage-ring requirements for luggage interrogation using tomographic imaging based on conventional storage-ring design. Based on scaling and reasonable parameter values, we conclude that it is unlikely that a single storage ring of con-

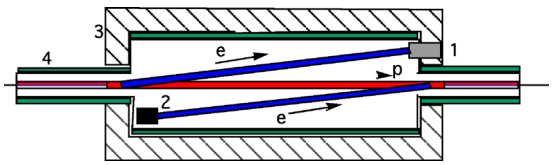

FIG. 14. (Color online) Electron and proton beams separation scheme in the dipole magnet. The electron beam moves from the source into the proton orbit. In the cooling section the electron and proton beams move together. Finally, in the next bending magnet the electron beam moves to the collector and is absorbed.

TABLE V. Preliminary storage-ring parameters.

Parameter	Value
Proton energy	1.75 MeV
Circumference (R=80 cm, L=150 cm)	11.0 m
Length of straight sections	150 cm
Average radius	1.75 m
Revolution frequency	1.66 MHz
Total length of cooling sections	about 420 cm
Electron current	about 1.0 A
Radius of bending magnet	80 cm
Transverse field in bending magnet (R=80 cm)	2.4 kG
Field index	0.5
Longitudinal magnetic field	25 kG
Electron beam radius	the same as proton beam radius
Aperture of vacuum chamber ∅	5–10 cm
Proton current	100 mA–1 A
Injection current (dc)	100–300 μA
Injected particle	H^0
Injection method	stripping on the internal target
Initial angular spread at injection	3 mrad
Initial energy spread of proton beam	±30 KeV
Target	CH_4 (methane)
Target density	up to 10^{16} cm^{-2}
Average energy losses in target	up to 40 eV per turn
Luminosity	up to 10^{35} cm^2 s^{-1}

ventional design would be able to provide the required proton-beam intensity for NRA applications. However, we found that for a carbon foil thickness of 20 μg/cm^2 or less, a practical NRA inspection complex having more than ten inspection stations is possible with no more than a few storage rings per station.

In our second study, we have tried to incorporate the new ideas of charge neutralization and adding a longitudinal magnetic field in the storage-ring design to increase the gamma-ray flux. We found that the use of electron cooling in a storage ring with an internal target strongly suppresses the degradation of proton beam quality. This makes it possible to achieve a flux of resonant gamma rays of about 5.0×10^8 gamma rays per second. This highly effective cooling process is made possible as a result of the space-charge neutralization of the electron beam. We also found that adding a longitudinal magnetic field to the storage rings may help to mitigate the excessive betatron tune shift caused by the required large proton current and small angular spread. Special efforts will have to be made to achieve a stable state of the beam-plasma system. Additional studies, both theoretical and experimental, are needed to prove that a storage ring based on these ideas is practical.

E. VITA for the detection of explosives based on NRA in nitrogen

To produce the high-intensity, high-quality, proton beam required by the NRA method a tandem accelerator is preferred over other electrostatic accelerators because its ion source and gamma-ray production target are at ground potential and its required operating voltage is only half of that required in single-ended accelerators.

Conventional electrostatic tandem accelerator designs have limited beam current potential.[21] In the conventional system, two accelerating columns based on ceramic tubes are connected to a high voltage power supply and the stripping target is located between them. This scheme has major disadvantages for operations that require currents of a few milliamperes:

- The stripper gas is pumped through the accelerating columns.
- Charge builds up on the inner surfaces of the high voltage electrodes and ceramic insulators due to the emission of secondary electrons and ions produced by the interaction of the high current beam with the residual vacuum. This buildup of charge will eventually lead to arcing and eventual breakdown of the ceramic insulating properties.

To circumvent these limitations, a new concept for an intense-beam proton tandem accelerator was conceived at the Budker Nuclear Physics Institute (BINP) in Novosibirsk, Russia: the VITA.

The basis of the VITA design is that it does not contain accelerating columns with ceramic insulation. Instead, vacuum insulation replaces the accelerating columns. High voltage is applied through an electrical feedthrough insulator (an arbitrarily remote distance from the accelerator beam channel) to the cylindrical electrodes and the charge-exchange stripper is located within the vacuum tank. The pumping of the stripper gas is realized, not through the accelerating columns, but through regions without solid insulation at high voltage potential.

An additional advantage of the VITA design is a wider range of choices of high-voltage gradient for the elements of the feedthrough insulator in comparison with the choice of high-voltage gradient for accelerating columns.

Figure 15 depicts the full-scale design of the NRA complex based on the vacuum insulated tandem accelerator. A negative hydrogen-ion beam is formed by the ion source 3 and injected into the accelerator through the low-energy beam tract (LEBT) 4. Acceleration proceeds up to one-half the design energy and the beam is stripped from H^- to H^+ ions in the charge-exchange stripper tube at the center of high-voltage electrode 5. After charge exchange, a proton beam is formed at the exit. The beam is accelerated to twice the voltage of the high-voltage electrode. The full-energy proton beam is transported through the high-energy beam tract (HEBT) 7 and interacts with the gamma-ray production target 8.

The high-voltage electrode of the tandem is surrounded by a system of shields at different potential to provide homogeneous distribution of the potential and prevent any full-voltage breakdowns.

The most important component of the accelerator is the high-voltage feedthrough insulator 2, connecting the high-voltage power supply (HVPS) 1 located in a tank filled with SF_6 gas (0.8 MPa) to the vacuum tank of the accelerator. The high-voltage feedthrough insulator can be located away from the region of the accelerated beam.

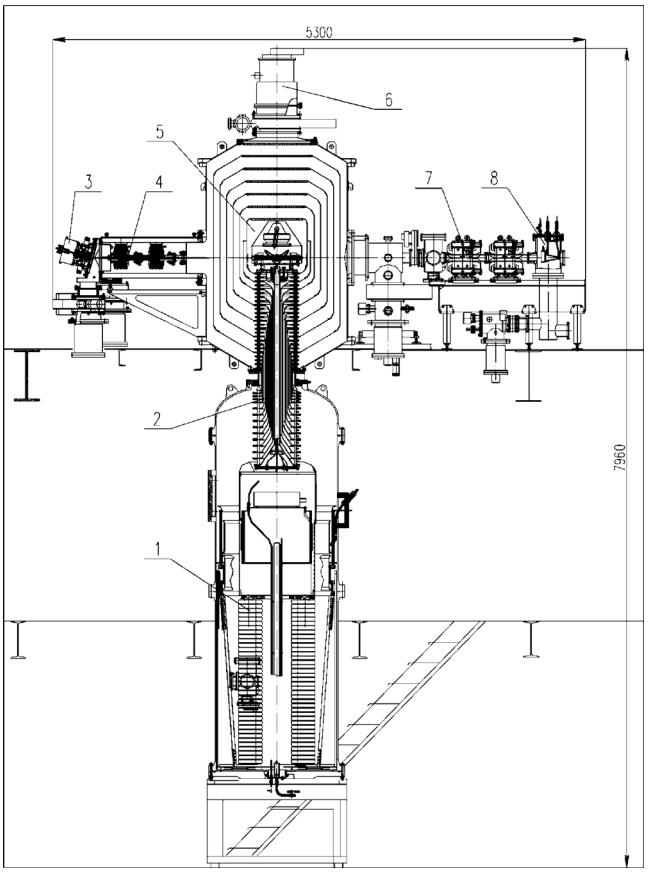

FIG. 15. VITA-based NRA complex.

The high-voltage electrode is at the vacuum end of the high-voltage feedthrough insulator, on the metal flange that is vacuum-sealed by the pipe passing along its axis. The pipe is connected to another metal flange placed at the pressurized-gas end of the insulator that is connected to the HVPS. The end of the high-voltage feedthrough insulator in the SF_6 is made up of a stack of ceramic rings separated by metal rings that distribute the potential. The end of the insulator located in the vacuum is made of glass rings, separated by metal rings. Thin-walled pipes of various lengths concentrically connect the metal rings of different potential on the SF6 gas end of the insulator to its counterparts within the vacuum. Voltage is applied to these rings through a resistive divider that distributes the potential homogeneously along the insulator.

The chosen electrostatic field intensity is 15 kV/cm across the separate insulators on the vacuum side of the high-voltage feedthrough insulator and 18 kV/cm for the insulators in the gas. Electrostatic intensity at the six accelerating gaps is 33 kV/cm. The stored energy in each high-voltage vacuum gap is limited to 30J.

Vacuum is maintained by cryogenic pump 6. Coaxial round holes for the passage of the beam are located in the walls of the vacuum tank, in the high-voltage electrode, and in the shields. Since the thin-walled shields are positioned along equipotential surfaces, the electrostatic field contributes slightly to focusing.

Argon gas was chosen for stripping the negative ion beam. The stripping target is a ~400-mm-long pipe with 10 mm diameter. Gas is supplied at a rate to produce a density of 3×10^{16} mol cm^{-2} as required for 99% stripping efficiency.

FIG. 16. (Color online) Vacuum tank.

Several stripper designs were considered:

(i) with external pumping through the heads of the equipotential shields,
(ii) with argon gas recycling using a turbo-molecular pump inside the high-voltage electrode.

High-voltage conditioning procedures, as well as high-voltage standoff of the vacuum gap, depend on the energy stored in capacitors before breakdown. When the machine starts up, high-voltage conditioning through cycling rf power in successively higher magnitudes is needed to avoid electrical breakdown for the acceleration of proton beams at an energy of 1.75 MeV and a current up to 1 mA. Figures 16–18 depict the major VITA subsystems.

FIG. 17. (Color online) Feedthrough insulator.

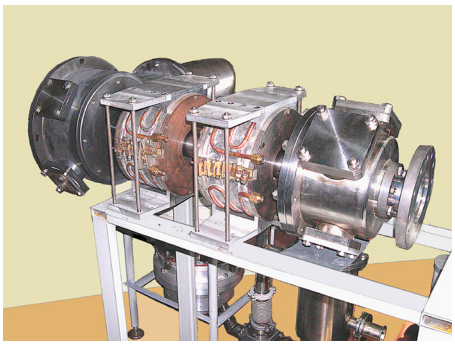

FIG. 18. (Color online) LEBT channel.

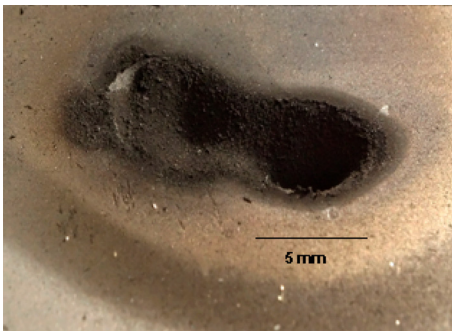

FIG. 19. (Color online) The first target after two experiments, operating about 10 min in the 1.8 MeV proton beam at 1 mA.

IV. USE OF ENABLING TECHNOLOGIES

A. High-power NRA target design and performance

1. Effects of high beam power

Several destructive factors threaten the operation and survival of the resonance absorption gamma-ray production target and require minimization. These include the influences of physical, chemical, and surface sputtering, and embrittlement. Experimental and theoretical research of graphite stability under the influence of a proton beam was studied in detail in previous works (for example, Ref. 12). Numerical calculations based on the Roth model,[22] where physical and chemical factors are considered as coexisting simultaneously, concluded that the region of optimum temperatures for a working target is in the range from 1100 to 2100 K for a proton beam energy up to 2 MeV.

Physical sputtering starts at proton energies higher than some minimum threshold, reaches a maximum, and then decreases as a function of the increase of proton range in graphite. Chemical sputtering, on the other hand, depends mainly on target temperature and reaches a maximum at target temperature $T \sim 800$ K, then decreases with increasing temperature due to thermal decomposition of hydrocarbons formed in the target. Surface sputtering, in turn, is caused by the accumulation of gases in the surface layer and its diffusion accompanying graphite decondensation. At target temperatures greater than 1100 K, the total rate of target sputtering will not exceed 0.5 μm per day.[23] It should be noted that synthesis of methane occurs at a target temperature lower than 1100 K, and acetylenes synthesizes at $T > 1100$ K, the output of which grows a little with the increase of the target temperature.

With the increase of the graphite temperature, its evaporation increases as well, so graphite vapor pressure reaches 1 atm at $T \sim 3700$ K. At working temperature of the target up to 2100 K, vapor pressure is too low to have a significant influence on vacuum conditions.

2. Target design and testing

Based on the above data, a thick graphite target was designed and fabricated with equal concentrations of carbon-12 and carbon-13. Secondary electrons were suppressed with a high-voltage suppressor. Resonant gamma rays are emitted through a thin copper window. Proton current on target is measured. Heat deposition on the target surface is calculated based on the measurements of temperature and cooling water flow.

Two targets were used in experiments, the first of which was exposed to a high power density ($\sim 3-5$ kW/cm^2). Scorches made by the proton beam on the target surface are shown in Fig. 19. Target temperature in the area of the beam was ~ 3000 K according to estimations, so the rate of graphite evaporation exceeded 2.6 μm/s.

This experience was taken into account in designing the second target which was located at a point in the beam line where an acceptable power density and surface temperature was achieved. The second target, shown in Fig. 20, has worked in a series of experiments totaling about 40 h at a proton beam current of ~ 200 μA. Surface sputtering appears to be insignificant.

B. NRA experimental measurements

1. NRA measurement apparatus

A gamma-ray spectrometer complex has been created (Fig. 21), including two scintillation detectors, positioned one over the other, inside a lead shield with ~ 10 cm wall thickness as well as two lead collimators directed at the carbon target.

A vessel containing liquid nitrogen is positioned such that gamma rays pass through the nitrogen and into one detector and miss the nitrogen in the other. To register the gamma rays attenuated by resonance absorption in nitrogen, the bismuth germanate $Bi_4GE_3O_{12}$ (BGO) scintillator detector is used; CsI is used as the other gamma-ray detector

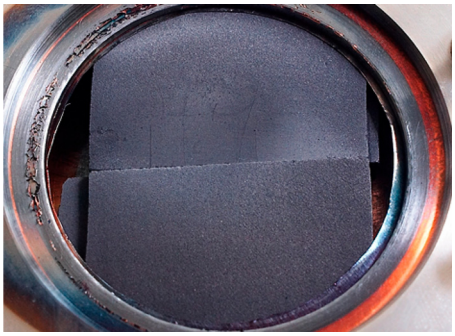

FIG. 20. (Color online) The second target after ~ 40 h in the beam at ~ 200 μA.

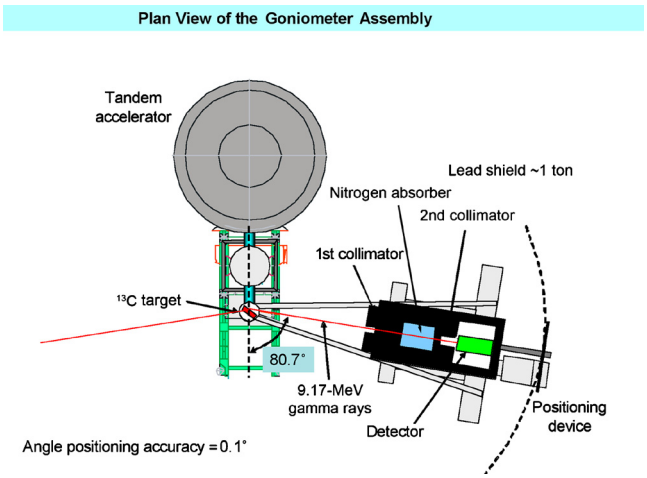

FIG. 21. (Color online) Experimental layout for resonant gamma absorption measurements.

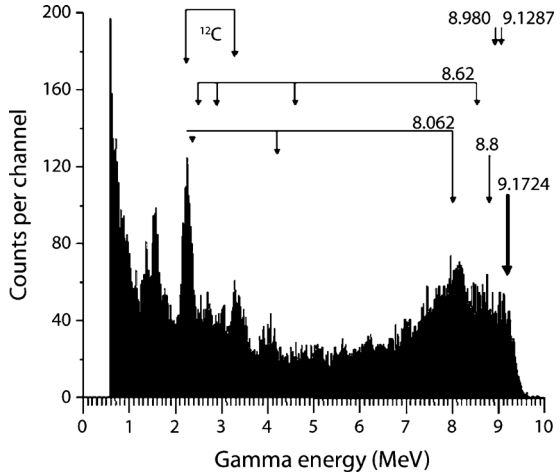

FIG. 23. Gamma-ray pulse-height distribution measured from a thick carbon-composite target at 1800 keV proton energy.

intended to continuously monitor the intensity of the proton beam on the target.

The entire system is placed on the goniometer, a mobile platform that rotates about an axis through the gamma-ray generating target. It provides for the measurement of both the resonant and nonresonant attenuation in the nitrogen by changing the angle. The accuracy of the goniometer rotation is approximately ~0.1°.

By gradually increasing the proton beam energy, the gamma rays associated with resonant production are encountered. Integrating the number of gamma rays in this 9.17 MeV region as the proton energy is increased through the resonant energy, an excitation curve for the given resonance is generated (Fig. 22). The threshold of the reaction is 1746.6 ± 0.9 keV, very narrow, indeed.[24] Thus, the slope of the excitation curve is defined entirely by the instability of the proton beam energy. As was established by the curve in Fig. 22, the proton energy resolution in the VITA beam is approximately ~1% of the average beam energy.

2. Results

A 2 MeV electrostatic proton tandem accelerator with vacuum insulation, originally developed to generate epithermal neutrons for boron neutron capture therapy of malignant tumors, has been used for explosive-detection experiments.[25,26] Using the 9.17 MeV gamma rays produced in the $^{13}C(p,\gamma)\ ^{14}N$ reaction, the gamma rays are resonantly absorbed in the nitrogen that constitutes most explosives.

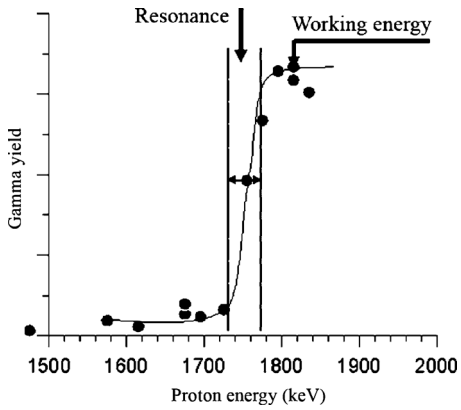

FIG. 22. Excitation curve for 9.17 MeV gamma rays from the reaction, $^{13}C(p,\gamma)\ ^{14}N$.

A thick carbon target made from graphite enriched in carbon-13 capable of withstanding a proton beam with high power density has been developed for generating the 9.17 MeV gamma rays. The diagnostic complex for detecting and analyzing the nitrogen-absorbing resonance gamma rays has been assembled and tested. It includes a goniometer with two collimators and lead-shielded gamma-ray detectors.

The spectrum of radiation generated by a thick carbon-13 target (Fig. 23) appears complicated, in addition to the gamma rays generated by carbon-12, which is also a major component of the target.

In the process of carrying out this work, a new method for normalizing the measured data was suggested—normalization by the 2.36 MeV gamma ray connected with the reaction $^{12}C(p,\gamma)\ ^{13}N$. This line appears far enough from the 9.17 MeV line and, therefore, has a little susceptibility to changes in the resonant gamma-ray output. At the same time, the output of 2.36 MeV gamma rays also depends directly on the intensity of the proton beam. Thus, this gamma ray can be used for normalizing the measured data because they are not resonantly absorbed in nitrogen. The transmission factor K, *then*, is the relation of the number of measured resonant γ-rays, N_r, to the number of measured non-resonant 2.36-MeV γ-rays, N_n.(Fig. 24).

The pulse-height distributions of the several gamma rays were measured and the transmission factor K was defined for different angular positions of the goniometer. A 38-cm-long vessel filled with either liquid nitrogen or water was placed in the path of the collimated beam of the γ-rays registered by the detector. For these two cases the dependence of the transmission factors K on the goniometer position is depicted in Fig. 25. Noticeable attenuation of the resonant γ-rays is observed at an angle around 80.7° when the vessel is filled with nitrogen. As observed in earlier experiments in our study, resonance attenuation of 9.17 MeV gamma rays is still detectable when the vessel length is scaled down to 7.5 cm.

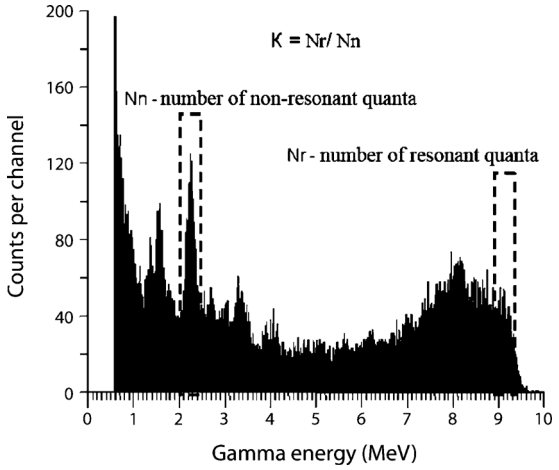

FIG. 24. Method of normalizing of the resonance gamma-ray intensity.

Thus, the results of the measurements presented here not only confirm the conclusions of previous research studies, but also show ways to improve the technique. First, it is shown that using a thick gamma-ray generating target simplifies its design and should increase the target lifetime. A more complicated distribution of gamma radiation in comparison with a thin target is not an absolute obstacle. Second, a new normalization method is suggested and tested experimentally. This method allows us to discard the second gamma-detector that naturally reduces measurement time.

V. CONCLUSIONS

Our analysis and computer simulations show that the use of electron cooling in the storage ring with internal target strongly suppresses the degradation of proton beam quality. This makes it possible to achieve a flux of resonant gamma rays of about 5.0×10^8 gamma rays per second. The effective cooling process is possible as a result of the space-charge neutralization of the electron beam. Special efforts will have to be made to achieve a stable state of the beam-plasma system. The requirement for large proton current and small angular spread leads to an inadmissible value of the betatron tune shift. The choice of the ring structure with longitudinal magnetic field may help to solve this problem. Development of the cyclotron-storage-ring accelerator system is technologically high-risk but high payoff, and it will require a dedicated experimental effort of significant magnitude to quantify critical issues such as electron cooling and proton beam stability in the storage ring. If such cyclotron-storage-ring system can be realized, this technology will open many new possibilities for applications of high-quality and high-averaged current proton beams. In the near term, the vacuum insulated tandem accelerator with an intense ion source holds a bright promise in the production of high-averaged current proton beams to generate active interrogation beams such as neutron and gamma for detection of explosives and SNMs. In our study, the vacuum insulated tandem accelerator at BINP achieved proton beams at energies up to 2.0 MeV and current up to 1.0 mA with an estimated emittance of 30π mm mrad. With the use of high frequency radiofrequency-power in the future, the footprint of such an accelerator can be reduced for compact applications.

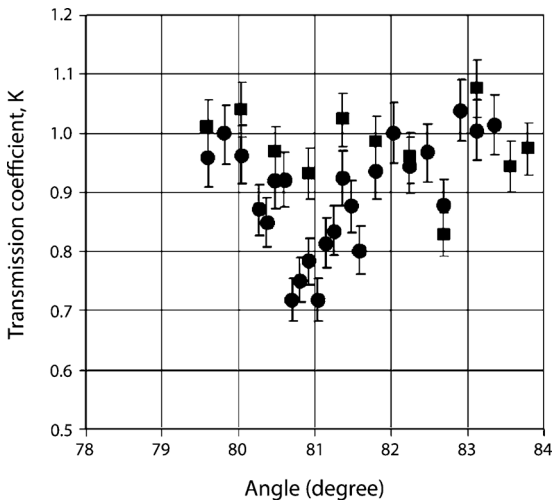

FIG. 25. Dependence of transmission coefficient K on the angle of the goniometer for liquid-nitrogen-filled vessel (squares) and water-filled vessel (circles).

ACKNOWLEDGMENTS

This work, supported by the Weapons Safeguards and Security Exchange (WSSX) program, was performed by Los Alamos National Laboratory operated by Los Alamos National Security, LLC, for the National Nuclear Security Administration of the U.S. Department of Energy under contract no. DE-AC52-06NA25396.

[1] R. E. Morgado, C. C. Cappiello, M. P. Dugan, C. A. Goulding, S. D. Gardner, C. L. Hollas, B. L. Berman, R. W. Hamm, K. R. Crandall, J. M. Potter, and R. A. Krauss, in *Proceedings of the SPIE Conference on Substance Detection Systems*, Insbruck, Austria, October 1993, Vol. 2092, pp. 503–513.
[2] D. Vartsky, M. B. Goldberg, G. Engler, A. Breskin, A. Goldschmidt, E. Izak, and O. Even, U.S. Patent No. 4,941,162 (10 July 1990).
[3] J. Brondo, L. Wielopolski, P. Thieberger, J. Alessi, D. Vartsky, and J. Sredniawski, AIP Conf. Proc. **680**, 931 (2003).
[4] A. Fessler, T. N. Massey, B. J. Micklich, and D. L. Smith, Nucl. Instrum. Methods Phys. Res. A **450**, 353 (2000).
[5] Handbook on Nuclear Activation Cross-Sections, IAEA Technical Report Series No. 156, International Atomic Energy Agency, Vienna, 1974.
[6] L. M. Onischenko, Yu. G. Alenitsky, A. A. Glazov, G. A. Karamysheva, D. L. Novikov, E. V. Samsonov, A. S. Vorozhtsov, S. B. Vorozhtsov, and N. L. Zaplatin, in *Proceedings of The XIX Russian Accelerator Conference (RuPAC2004)*, Dubna, Russia, 4–9 October 2004.
[7] R. L. Macklin and J. H. Gibbons, Phys. Rev. **109**, 105 (1958).
[8] B. F. Bayanov, V. P. Belov, E. D. Bender, M. V. Bokhovko, G. I. Dimov, V. N. Kononov, O. E. Kononov, N. K. Kuksanov, V. E. Palchikov, V. A. Pivovarov, R. A. Salimov, G. I. Silvestrov, A. N. Skrinsky, N. A. Solov-iov, and S. Yu. Taskaev, Nucl. Instrum. Methods Phys. Res. A **413**, 397 (1998).
[9] D. L. Novikov (private communication).
[10] S. B. Vorozhtsov, E. E. Perepelkin, and L. M. Onischenko, "Customs cyclotron and beam delivery system," in *Proceedings of The 18th International Conference on Cyclotrons and their Applications Cyclotrons 2007*, Laboratori Nazionali del Sud, Giardini Naxos, Italy, October 2007.
[11] G. Dimov, V. Shamovskii, and V. Chupriyanov, Sov. Phys. Tech. Phys. **16**, 1662 (1972).
[12] L. A. Ferrari and M. S. Zucker, Phys. Fluids **12**, 1312 (1969).
[13] T. F. Wang and T. J. T. Kwan, "A study of storage ring requirements for an explosive detection system using NRA methods," in *Proceedings of the 2005 Particle Accelerator Conference*, Knoxville, TN (2005), Vol 2.
[14] T. F. Wang and T. J. T. Kwan, Los Alamos National Laboratory Report No. LA-UR-04–5457, 2004.

[15] V. V. Parkhomchuk, V. B. Reva, V. A. Vostikov, and V. F. Dimitriev, "Theoretical investigation and computer simulation of the storage ring with electron cooling of proton beam and compensation of target influence," BINP Report, 2005.
[16] R. E. Morgado, G. Arnone, C. C. Cappiello, S. D. Gardner, C. L. Hollas, L. E. Ussery, J. M. White, Z. D. Zahrt, and R. A. Krauss, Los Alamos National Laboratory Report No. LA-12776-MS, 1994.
[17] See http://mad.home.cern.ch/mad for MAD-X.
[18] A. Smirnov, A. Sidorin, and G. Trubnikov, "Description of software for BETACOOL program based on BOLIDE interface," JINR Report, 2004.
[19] G. Dimov, V. Dudnikov, and V. Shamovskii, J. Tech. Phys. **41**, 2028 (1971).
[20] G. Budker, Ya. S. Derbenev, N. Dikansky, V. Kudelainen, I. N. Meshkov, V. V. Parkhomchuk, D. V. Pestrikov, B. N. Sukhina, and N. N. Skrinsky, IEEE Trans. Nucl. Sci. NS–22 (1975).
[21] V. V. Parkhomchuk and A. N. Skrinsky, Rep. Prog. Phys. **54**, 919 (1991).
[22] V. Kudelainen, V. Parkhomchuk, and D. Pestrikov, J. Tech. Phys. **53**, 870 (1983).
[23] B. F. Milton, "A high current tandem accelerator for gamma-resonance contraband detection," in *Proceedings of the Particle Accelerator Conference*, Vancouver, Canada, 1997.
[24] V. T. Astreliin, A. V. Burdakov, P. Z. Chebotaev, V. V. Filippov, V. S. Koidan, K. I. Mekler, P. I. Melnikov, V. V. Postupaev, A. F. Rovenskikh, M. A. Shcheglov, and H. Wuerz, Nucl. Fusion **37**, 1541 (1997).
[25] L. Barkov, G. Derebyankin, G. Dimov, G. Kraynow, A. Krivenko, S. Fadeev, V. Shirokov, G. Silvestrov, I. Sorokin, S. Taskaev, and M. Tiunov, Proceedings of EPAC 2002, Paris, France, 2002, p. 852.
[26] A. Burdakov, V. Davydenko, V. Dolgushin, A. Dranichnikov, A. Ivanov, J. P. Farrell, A. Khilchenko, V. Kobets, S. Konstantinov, A. Krivenko, A. Kudryavtsev, M. Tiunov, V. Savkin, V. Shirokov, and I. Sorokin, Nucl. Instrum. Methods Phys. Res. B **261**, 286 (2007).